01 Mar 2022

Revealing Bluff-Body Aerodynamics on Low-Rise Buildings under Tornadic Winds using Numerical Laboratory Tornado Simulator

Ryan Honerkamp

Guirong Grace Yan
Missouri University of Science and Technology, yang@mst.edu

John Van De Lindt

Recommended Citation

R. Honerkamp et al., "Revealing Bluff-Body Aerodynamics on Low-Rise Buildings under Tornadic Winds using Numerical Laboratory Tornado Simulator," *Journal of Structural Engineering (United States)*, vol. 148, no. 3, article no. 04021294, American Society of Civil Engineers, Mar 2022.
The definitive version is available at https://doi.org/10.1061/(ASCE)ST.1943-541X.0003283

ASCE

Revealing Bluff-Body Aerodynamics on Low-Rise Buildings under Tornadic Winds Using Numerical Laboratory Tornado Simulator

Ryan Honerkamp, Ph.D., M.ASCE[1]; Guirong "Grace" Yan, F.ASCE[2]; and John van de Lindt, F.ASCE[3]

Abstract: Tornadoes result in death and property loss in communities around the world. To quantify the actions of tornadoes on civil structures, researchers have built physical laboratory tornado simulators to simulate tornadoes in the lab environment and tested building models in the simulated tornadic wind field, which is similar to wind tunnel testing when quantifying the wind effects induced by straight-line winds. Unfortunately, physical tornado simulators are much less common than straight-line wind tunnels, leading to the lack of research on bluff-body aerodynamics on civil structures under tornadic winds. Considering that it is expensive to conduct experimental testing in physical tornado simulators, numerical models of physical tornado simulator has been developed using computational fluid dynamics (CFD) simulations. However, they have not been validated at the level of pressure distribution on the structural surface of the testing model. In this study, the numerical model developed for the large-scale tornado simulator of the Missouri University of Science and Technology (Missouri S&T), which is based on the numerical simulation of the entire process of the physical testing in tornado simulator, will be validated by the measured data on the building model tested in the physical tornado simulator. Then, through the validated numerical simulation model, the bluff-body aerodynamics of buildings under tornadic winds will be revealed. To be specific, CFD simulation is first applied to model the entire process of experimental testing of a low-rise building model in the physical tornado simulator. Then, the obtained results are compared with laboratory-measured data to evaluate the effects of the building model on the wind field and the surface pressure on the building model. Then, the bluff-body aerodynamics on low-rise buildings under tornadic winds will be revealed based on the data obtained from numerical simulations using the relationship between streamline pattern change and velocity magnitude change (mass continuity theorem) and using the relationship between the velocity magnitude change and the pressure change (Bernoulli's theorem), as well as the flow separation and vortex shedding.
DOI: 10.1061/(ASCE)ST.1943-541X.0003283.

Author keywords: Tornado-like vortex; Computational fluid dynamics (CFD); Structure; Bluff-body aerodynamics.

Introduction

Tornado-induced injuries, deaths, and property loss occur around the world every year, especially in the United States, where 1,200 tornadoes occur annually (NOAA 2019). On average, 90 deaths and 1,500 injuries occur in the United States annually as a result of tornadoes, and the related average annual property loss is estimated as $1 billion (Simmons et al. 2013; Changnon 2009). To minimize the tornado-induced fatalities and property loss, it is important to build more wind-resistant civil structures, which requires an in-depth understanding of the wind effects of tornadoes on civil structures.

Research into tornadic wind effects on civil structures relies heavily on wind characteristics near the ground, but unfortunately, near-ground wind fields during tornadoes are rarely reported due to the violent and short-lived nature of tornadoes and the limitations of radar measurement (Snyder and Bluestein 2014). Therefore, laboratory simulation of tornadoes in a controlled environment is one of the safest ways to study how the flow field is altered by the presence of civil structures and the corresponding wind effects on civil structures. Thus far, several laboratory tornado simulators have been built (Mishra et al. 2008; Haan et al. 2008; Rajasekharan et al. 2013; Refan and Hangan 2016), and wind effects of tornado-like vortices on several archetypes of civil structures have been studied in the lab (Mishra et al. 2008; Rajasekharan et al. 2013; Haan et al. 2010). However, physical laboratory simulators can be cumbersome to operate, financially costly to implement, and physically space-consuming in order to achieve higher accuracy measurements. Specifically, tornado simulators are often plagued by skepticism based on the issue of measurement resolution. This means that smaller simulators are viewed as less accurate, but larger simulators are expensive, leading to a conundrum. In either situation, how the flow field is altered by the presence of civil structures requires particle image velocimetry (PIV) measurement, which is extremely expensive. To try to address these problems, the laboratory tornado simulators have been numerically simulated (Kuai et al. 2008; Liu and Ishihara 2015; Yuan et al. 2019). However, the numerical simulation is often simplified to reduce computational demand, which may consequently produce deficiencies in the final results. Therefore, the present authors have improved the numerical simulation of the laboratory tornado simulator by modeling all mechanical components in the physical tornado simulator.

[1]Dept. of Civil, Architectural, and Environmental Engineering, Missouri Univ. of Science and Technology, Butler-Carlton Hall, 1401 N Pine St., Rolla, MO 65409. Email: rh7v7@mst.edu

[2]Associate Professor, Dept. of Civil, Architectural, and Environmental Engineering, Missouri Univ. of Science and Technology, Butler-Carlton Hall, 1401 N Pine St., Rolla, MO 65409 (corresponding author). Email: yang@mst.edu

[3]Professor, Dept. of Civil and Environmental Engineering, Colorado State Univ., Engineering Bldg., 1372 Campus Delivery, Fort Collins, CO 80523. Email: jwv@engr.colostate.edu

Note. This manuscript was submitted on July 3, 2021; approved on October 27, 2021; published online on December 24, 2021. Discussion period open until May 24, 2022; separate discussions must be submitted for individual papers. This paper is part of the ***Journal of Structural Engineering***, © ASCE, ISSN 0733-9445.

In the previous studies on the simulation of laboratory tornado simulators, the focus was to study the wind characteristics of the tornadic wind field. If the numerical simulation could model the experimental testing in the tornado simulator, that is, find the wind pressure distribution on the testing model using numerical simulation, systematic experimental testing for many cases can be conducted numerically. By doing this, because computational fluid dynamics (CFD) simulation can provide data at any desired resolution technically, the resolution limitation in experimental testing will be addressed and the flow pattern change due to the presence of civil structures can be easily obtained. After a comprehensive literature review, no studies have been reported on studying tornadic wind effects on civil structures in a "numerical" laboratory tornado simulator; no studies have been reported to validate the numerical simulation of laboratory tornado simulator using the pressure distribution on the surface of a structural model measured in the physical tornado simulator (previous studies used the velocity and pressure data in the wind field for validation). In addition, bluff-body aerodynamics of a building model under tornadic winds has not been performed.

To bridge these research gaps, this study investigates the wind effects of tornado-like vortices on low-rise buildings through numerically modeling the experimental testing of the structural model in the laboratory tornado simulator, which will be validated using the measurements obtained from the laboratory tornado simulator. To be specific, a small-scale model of a gable-roofed building will be placed in the "numerical" laboratory tornado simulator and CFD simulations will be performed to investigate how the tornadic wind flow is diverted around the building and to provide wind pressure distribution on the building surface and total forces/moments acting on the entire building. The obtained wind effects will be validated through the testing data measured from lab testing in the physical laboratory tornado simulator, which has been published in Haan et al. (2010). Then, the bluff-body aerodynamics on low-rise buildings under tornadic winds will be revealed based on the data obtained from numerical simulations. The remainder of this paper is structured as follows. First, the CFD simulation setup is presented with a convergence study. Second, the results of the numerical simulation are presented and discussed in comparison with the physical results. Third, final conclusions are drawn, and future research is suggested.

CFD Simulation Setup

The physical laboratory tornado simulator at Missouri S&T is considered here, as shown in Fig. 1. Its numerical model developed in Yuan et al. (2019) is adopted here. All walls/floors/solid sections in the physical laboratory simulator, are set as no-slip walls in the numerical simulation. The fan is simulated as a fan interface, modeled as a pressure jump, and the honeycomb section under the fan interface is modeled using a porous media zone, as shown in Fig. 1(a). More details on the related setup can be referred to (Yuan et al. 2019).

In this study, the small-scaled (with the scale of 1:100) model of a gable-roofed building [see Fig. 1(d)] is placed in the computational domain. Large-eddy simulation (LES) that is governed by the filtered Navier–Stokes (N–S) equation is applied to solve large eddies, while small eddies are numerically modeled by a Smagorinsky-Lilly subgrid model. Pointwise is used to generate the mesh, with coarser mesh in the upper domain and finer mesh near the ground and around the building model. Then, the mesh is imported into ANSYS FLUENT for solving with a finite volume-based SIMPLEC solution scheme [(Fluent Manual 2017a) "Large Eddy Simulation"]. Following the convergence study, the following cell density was achieved near the ground away from the building model the mesh size is much coarser as these locations are not of

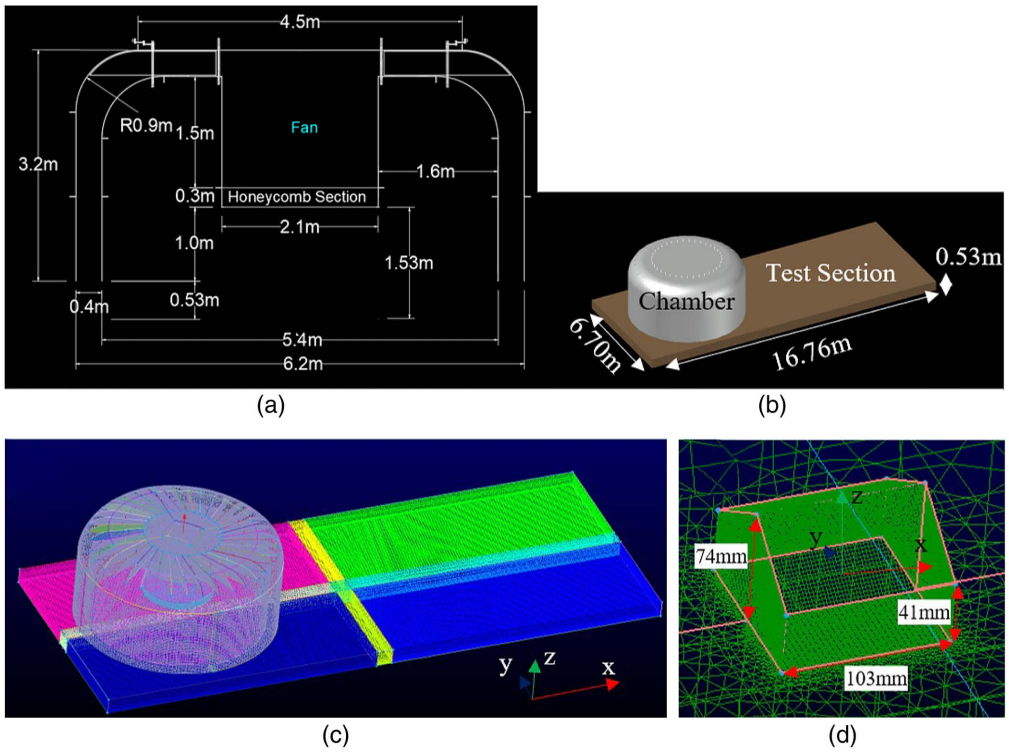

Fig. 1. Laboratory tornado simulator at Missouri S&T: (a) major dimensions of the vortex-generating chamber; (b) dimensions of physical facility test section; (c) meshing of the computational domain; and (d) the building model tested in the numerical simulator.

particular interest for surface pressure investigation, roughly 0.025 m × 0.025 m (1 in. X 1 in.), with a logarithmic inflation technique where the first layer is 0.013 m (0.5 in.). In the vicinity of the building and on the structural surface the meshing is much finer, as shown in Fig. 1(d). Specifically, on the building surface, the mesh is 0.002 m × 0.002 m with the first layer being 0.001 m and increasing logarithmically.

In order to accurately determine the pressure in the computational domain, it is necessary to set the reference pressure location far away from the center of the tornado-like vortex. For this simulation, the reference pressure location was set at the bottom edge of the test section, as shown in Fig. 2. At this location, the pressure is set to be atmospheric pressure, meaning that the pressure outside the vortex-generating chamber would be atmospheric, as swirling wind flow is generated through self-circulation (recirculation) of the air inside the chamber and thus the vortex is formed inside the chamber with minimal, if any, interference from the air outside.

The simulation is first run in a stationary case (where the vortex-generating chamber does not move) for 5 s to form the vortex; then, the simulation is switched to a translating case (the vortex-generating chamber moves) until the generated vortex passes over the building model. The simulation time step is 0.01 s/step. The following parameters are taken from the physical experiment reported in Haan et al. (2010). The length scale is set as 1:100 and the time scale is 1:13.8. The vane angle of the simulator model is set up as 15° and the uniform height from the ground plane to the bottom of the simulator is set as 0.53 m (corresponding to 53 m in full-scale). The test section where the building models are placed, as shown in Fig. 1(b), is 16.76 m long (corresponding to a 1,676 m translation path in full-scale). The fan power level is set to be 33%, which corresponds to a pressure jump of 131 Pa (0.019 psi) at the fan interface. The following two translating speeds (T) are applied, 0.15 m/s (0.34 mph) and 0.61 m/s (1.36 mph), which correspond to the two experimental setups from the physical testing conducted in the laboratory tornado simulator in (Cases 1 and 4 from Haan et al. 2010). The case with T = 0.61 m/s (1.36 mph) is used for the convergence study and the case with T = 0.15 m/s (0.34 mph) is used for the validation of results and for the exploration of bluff-body aerodynamics on civil structures under tornadic winds.

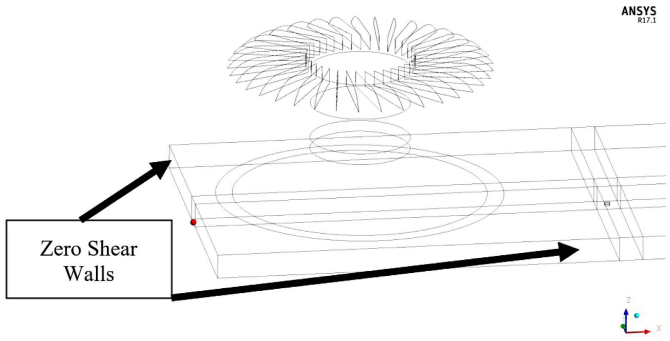

Fig. 2. Dot in lower left of box is the reference pressure location. Lower domain boundaries set as zero shear walls.

Table 1. Convergence study on mesh densities

Variable	Case 1: coarse	Case 2: medium	Case 3: fine
Cell count	8.3 million	8.5 million	9.3 million
r_1 (m)	0.27	0.27	0.28
$V_{\theta max}$ (m/s)	8.20	8.62	7.68
Q (m^3/s)	20.38	20.42	20.04
S	0.09	0.09	0.09

In order to determine mesh quality and refinement requirements, a convergence study is performed using three levels of mesh density, which are coarse, medium, and fine, as shown in Table 1. A comparison was made between the three cases with different mesh densities in the stationary situation when the generated tornadic wind flow is far away from the building model. As shown in Table 1, the identified core radius and Swirl Ratio in all three cases are almost identical. The Swirl Ratio (S) is determined using Eq. (1) (Haan et al. 2008)

$$S = \frac{\pi r_1^2 V_{\theta max}}{Q} \tag{1}$$

where r_1 denotes the core radius where maximum tangential velocity is found, $V_{\theta max}$ denotes the maximum tangential velocity, and Q denotes the volume flow rate through the simulator. Figs. 3 and 4 present time-averaged pressure contours on a vertical plane through the center of the simulator and on a horizontal plane near the ground of the test section, respectively. The maximum negative pressures are within 4 Pa (5.8×10^{-4} psi) of one another in each of the simulated cases. Fig. 5 presents contours of tangential velocity on a vertical plane through the center of the simulator, and Fig. 6 presents normalized tangential velocity profiles at different elevations above the ground in the testing section, where the tangential velocity is normalized by the maximum tangential velocity, the

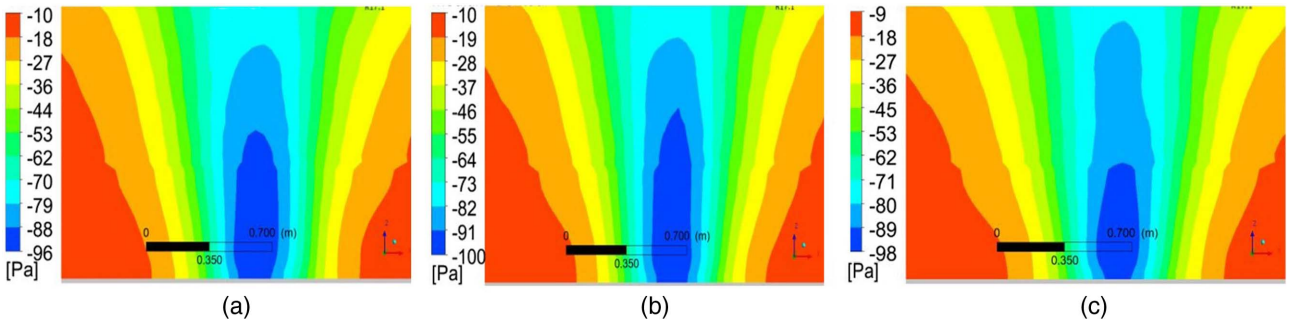

Fig. 3. Contours of pressure on a vertical plane through the center of the tornado simulator, directly under the honeycomb section [in Fig. 1(a), it is the square plane that is 2.1 m wide and 1.53 m tall under the honeycomb section], where the tornado-like vortex is generated after a 5-s spin-up. All figures are based on the results that are time-averaged over two seconds from t = 5 s to t = 7 s, with a sampling rate of 100 Hz: (a) coarse mesh; (b) medium mesh; and (c) fine mesh.

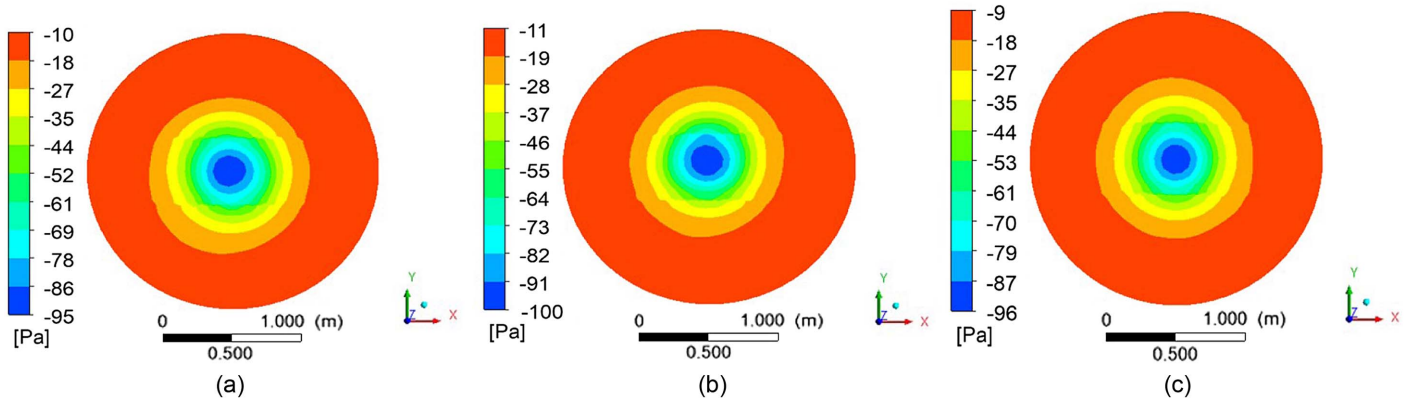

Fig. 4. Contours of pressure on a horizontal plane through the tornado simulator, directly under the fan at an elevation of 5 cm above the ground plane (i.e., very near the ground), where the tornado-like vortex is generated after a 5-s spin-up. All Figs. are time-averaged over two seconds from t = 5 s to t = 7 s, with a sampling rate of 100 Hz: (a) coarse mesh; (b) medium mesh; and (c) fine mesh.

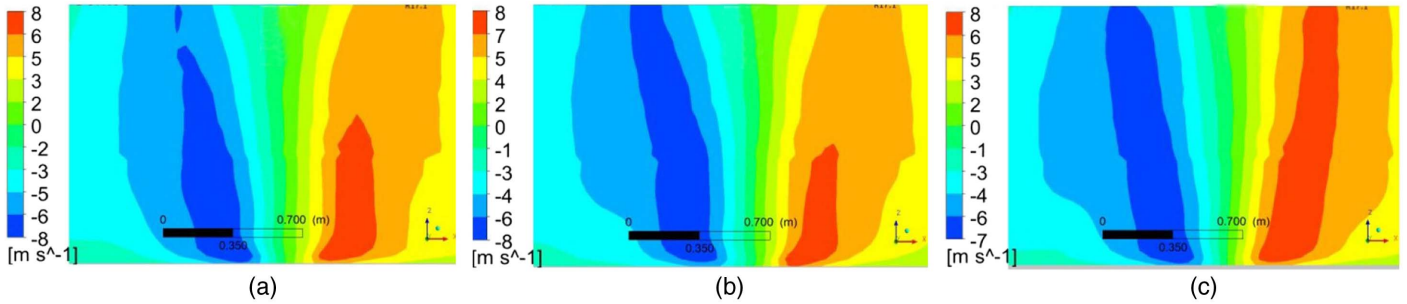

Fig. 5. Contours of tangential velocity on a vertical plane through the center of the tornado simulator, directly under the honeycomb section [in Fig. 1(a), it is the square plane that is 2.1 m wide and 1.53 m tall], where the tornado-like vortex is generated after a 5-s spin-up. All Figs. are the results that are time-averaged over two seconds from t = 5 s to t = 7 s, with a sampling rate of 100 Hz: (a) coarse mesh; (b) medium mesh; and (c) fine mesh.

radial distance is normalized by the core radius where the maximum tangential velocity is found (designated as R_{core} in this study), and the elevation is normalized by the height at which the core radius R_{core} is found. The tangential velocities and the tangential velocity profiles are nearly identical with all three mesh densities. As the fine mesh requires extensively longer computational time, for conceivably similar results, the coarse and medium meshes are selected for the following simulations.

Following the comparison for the stationary stage, the translating stage was simulated for the "coarse" and "medium" cases for comparison, where the tornado vortex translates at 0.61 m/s (1.36 mph) to the right. The sliding mesh technique is implemented here [(Fluent Manual 2017b) "Sliding Mesh Technique"] to simulate the translating of the generated tornado vortex, with the chamber moving while the test section and building model remain stationary. Considering that the building experiences the highest tangential velocity when the building is located at the core radius (Fig. 7), the results when the core radius of the tornado vortex passes the building are extracted and compared between the two cases with different meshing densities.

Based upon the tangential velocity distribution obtained, as shown in Fig. 7, the "coarse" mesh resulted in a slightly larger core radius, making the vortex reach the building model sooner in the "coarse" case. Comparing the "medium" and "coarse" mesh cases in terms of tangential velocity on a vertical plane, as shown in Fig. 7, it is seen that the "medium" mesh resulted in a slightly more detailed contour than the "coarse" mesh, which is evidenced by the small fluctuations captured inside the core radius {the irregular points on and above the roof ridge in Fig. 7(a)]}. This is due to the higher resolution in the "medium" mesh case. Fig. 8 presents the instantaneous wind pressure on the building model (referred to as "surface pressure") when the core radius of the tornado vortex passes the building model. Comparing the surface pressure distributions, negative pressure dominates in both cases and the peak negative pressure values are −168 Pa (0.024 psi) and −162 Pa (0.023 psi) for the cases with "medium" and the "coarse" mesh, respectively, with a 4% difference. Considering that the higher resolution in the "medium" mesh case resulted in finer resolution in the pressure distribution, the results presented in the following are based on the "medium" mesh density.

Results and Discussion

To reveal bluff-body aerodynamics on low-rise buildings under tornado-like vortices, the case where the tornado simulator translates at 0.15 m/s (0.34 mph) from the left to the right is simulated. This translating speed [0.15 m/s (0.34 mph)] corresponds to Case 1 in experimental testing conducted in the physical tornado simulator at Iowa State University (ISU) [the testing results were

J. Struct. Eng., 2022, 148(3): 04021294

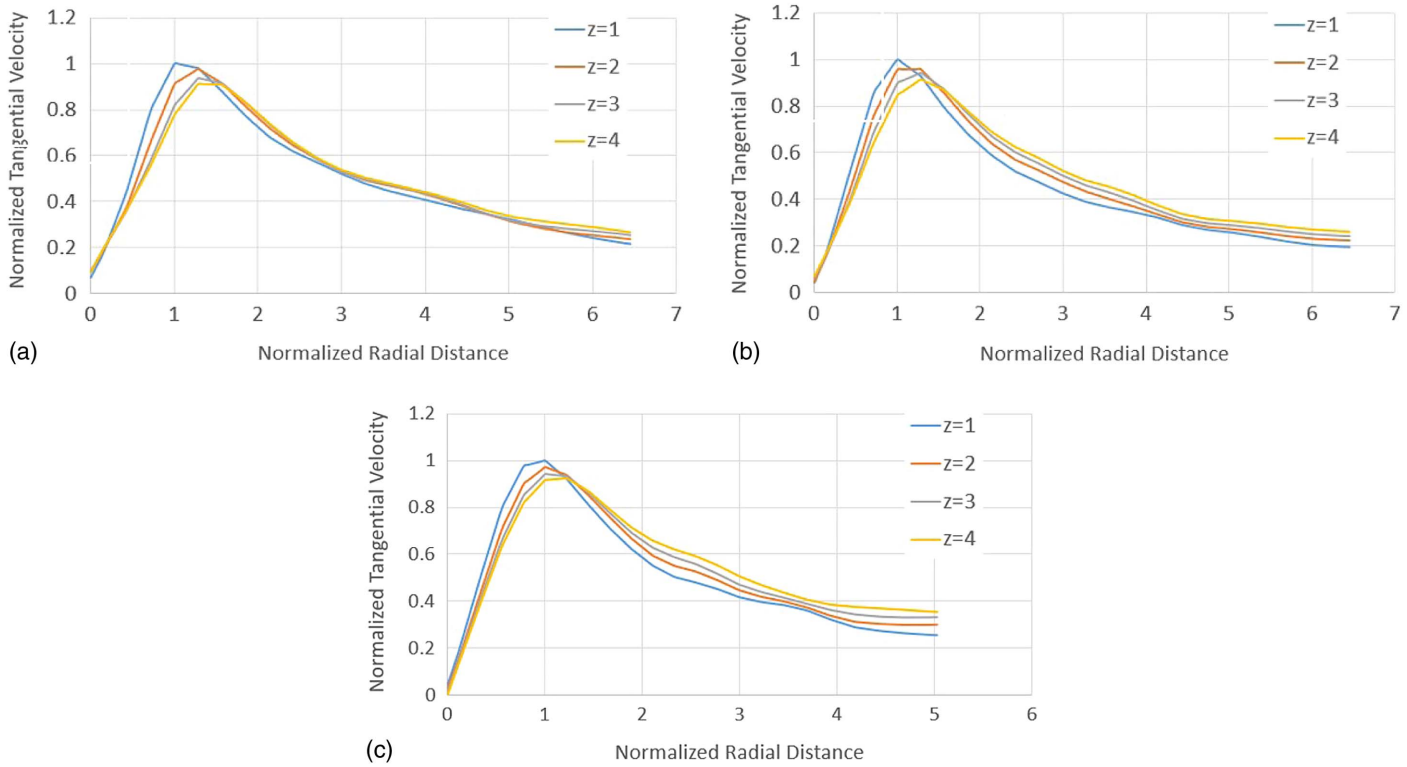

Fig. 6. Normalized tangential velocity profiles at four different elevations above the ground in the testing section. All Figs. are based on the results that are time-averaged over two seconds from t = 5 s to t = 7 s, with a sampling rate of 100 Hz: (a) coarse mesh; (b) medium mesh; and (c) fine mesh.

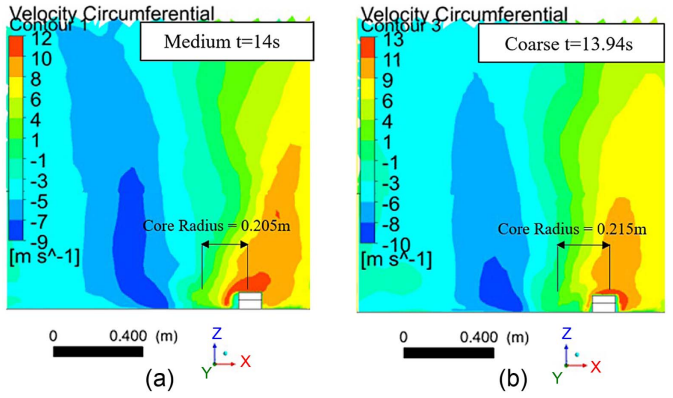

Fig. 7. Contours of tangential velocity on a vertical plane through the center of tornado simulator, directly under the honeycomb section [in Fig. 1(a), it is the square plane that is 2.1 m wide and 1.53 m tall under the honeycomb section], when the core radius passes the building model. Both are instantaneous at the time instants shown: (a) medium mesh; and (b) coarse mesh.

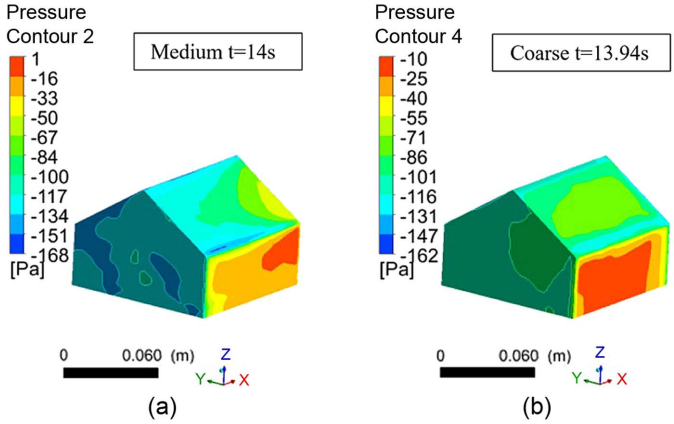

Fig. 8. Contours of surface pressure on the windward side of the building model, when the civil structure is located at the core radius. Both are instantaneous at the time instants shown: (a) medium mesh; and (b) coarse mesh.

published in Haan et al. (2010)], and thus comparison can be made to validate the numerical simulation before conducting systematic analyses of the results, as the tornado simulator of Missouri S&T is still under construction. The tornado simulator at Missouri S&T follows the same mechanism to generate swirling wind flow, although the size of the chamber at Missouri S&T is 17% bigger and some modifications were made for improving the efficiency of the facility (e.g., the extension of the turning vanes from the edge of the fan all the way to the edge of the outer shell, the curved top of the outer shell, and the increased capacity of the fan). This justifies that the numerical results presented here for the Missouri S&T simulator can be validated pre-emptively by using the dimensionless results obtained from the tests in the tornado simulator of ISU published in Haan et al. (2010).

To facilitate the comparison, force, moment, and pressure coefficients are used. The equations for converting the extracted forces (F_x, F_y, F_z) into force coefficients in the x-, y-, and z-directions (axes specified in Fig. 1), f_x, f_y, and f_z, respectively, are given by Eqs. (2), (4), and (6), respectively; the equations for converting

moments (M_x, M_y, M_z) into moment coefficients about the x, y, and z axes, m_x, m_y, and m_z, are given by Eqs. (3), (5), and (7), respectively; and the equation for converting surface pressure (P) into pressure coefficient (p) is given by Eq. (8). In the equations for f_x, f_y, m_x, and m_y, the same value of A is used, which is the product of the longest horizontal dimension of the model and the height of the roof ridge. A_z is the projected area of the building model on the horizontal plane, perpendicular to the z-direction; ρ is the air density; H is the mean roof height; V is the maximum horizontal resultant velocity; L is the longest horizontal dimension of the building model; P is the pressure in the computational domain adjacent to the building surface and is treated as the pressure on a structural surface; and P_∞ is the atmospheric pressure. Herein, the forces in the x-, y-, and z-directions acting on the geometric centroid of the building model are found by integrating the pressure on the building surface in that respective cardinal direction. Moments acting on the building model are calculated about the geometric centroid of the building bottom. For example, for the moment about the x-axis, the resultant force acting on the building in the y- and z-direction are multiplied by their respective eccentricities (vertical distance) from the building centroid to the ground and summed to determine the overall moment

$$f_x = \frac{F_x}{\frac{1}{2}\rho V^2 A} \tag{2}$$

$$m_x = \frac{M_x}{\frac{1}{2}\rho V^2 A H} \tag{3}$$

$$f_y = \frac{F_y}{\frac{1}{2}\rho V^2 A} \tag{4}$$

$$m_y = \frac{M_y}{\frac{1}{2}\rho V^2 A H} \tag{5}$$

$$f_z = \frac{F_z}{\frac{1}{2}\rho V^2 A_z} \tag{6}$$

$$m_z = \frac{M_z}{\frac{1}{2}\rho V^2 A_z L} \tag{7}$$

$$p = \frac{P - P_\infty}{\frac{1}{2}\rho V^2} \tag{8}$$

Validation Using Published Lab Testing Results

Figs. 9 and 10 present the variation of (instantaneous) force coefficients and moment coefficients as the tornado vortex passes the building model, respectively, zoomed in to better view the coefficient peaks. Due to the nonstationary nature of the tornado-like vortex when translating, the instantaneous values are presented. The horizontal axis represents the normalized distance from the center of the building model to the center of the vortex, designated here as "x/D", where D denotes the diameter of the core vortex in the stationary case at the elevation where the maximum tangential velocity occurs (0.5 m), i.e., 2 times the core radius. This normalization is consistent with that used in Haan et al. (2010).

From Fig. 9, f_x and f_y present peak values when the core radius of the vortex passes the building model; the sign convention (+/−) changes (the force direction changes) at the center of the vortex because the direction of radial velocity and tangential velocity change into the opposite direction when the vortex center passes the building model. f_x ranges between −1.0 and 1.4. f_y ranges between −1.5 and 1.25. f_z presents greater values when the core of the vortex passes the building model. In addition, the magnitude of the peak value of f_z, 2.5, is much greater than that of the peak values of f_x and f_y. This is evidenced further by the total force coefficient trend following the behavior of f_z more closely in the core region, shown as the "total" graph in Fig. 9.

From Fig. 10, the peak m_z is 0.16 and the peak m_x and m_y are 0.2 and 0.1, respectively. In Haan et al. (2010), the moment coefficients were only presented as a range of values. In all the setups that they ran, using different parameters, the peak values for m_z ranged from 0.04 to 0.3 and the peak values for m_x and m_y ranged up to 1.1 and 0.7, respectively. This means that the values for moment coefficients obtained from this numerical simulation are reasonable compared to the overall values from multiple setups in Haan et al. (2010). Fig. 11 presents the averaged force coefficients over one-second periods. As the numerical simulation proceeds through the solution, the program outputs values for the specified variables, pressures, velocity, temperature, etc., for each time instant/step that is specified, in this instance every 0.01 s. The moving average with 50% of data overlap is applied here. Because the time step is 0.01 s, the average over 1 s is based on 100 data points. Each data point in Fig. 11 is associated with the time instant when the building model moves to a certain location, and it is the averaged value based on the data 0.5 s (or 50 steps of data) back and

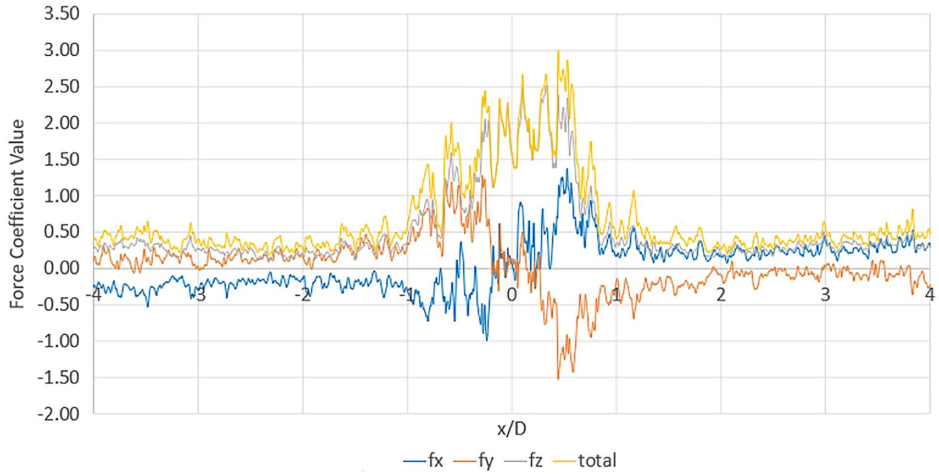

Fig. 9. Instantaneous force coefficients on the small-scaled model of the gable-roofed building versus distance from the center of the vortex to the center of the gable-roofed building model normalized by the core diameter (D). Zoomed in on the range of x/D from −4 to 4.

J. Struct. Eng., 2022, 148(3): 04021294

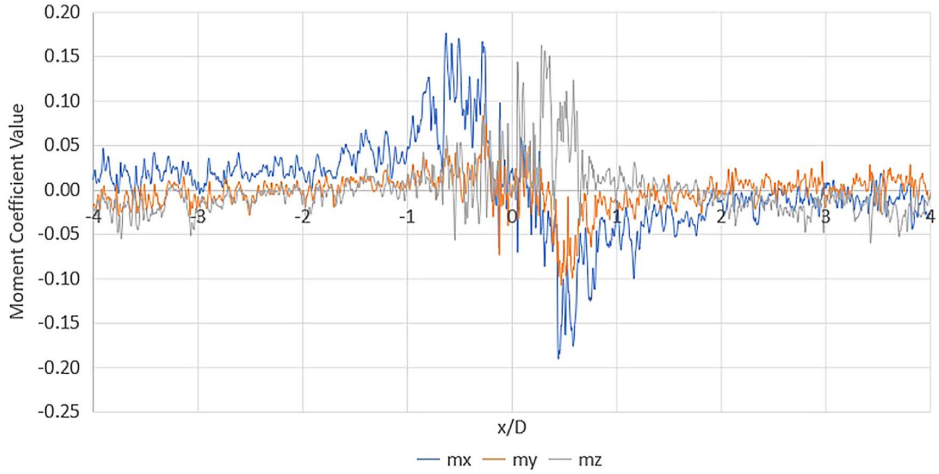

Fig. 10. Instantaneous moment coefficients on the small-scaled model of the gable-roofed building versus distance from the center of the vortex to the center of the gable-roofed building model normalized by the core diameter (D). Zoomed in on the range of x/D from −4 to 4.

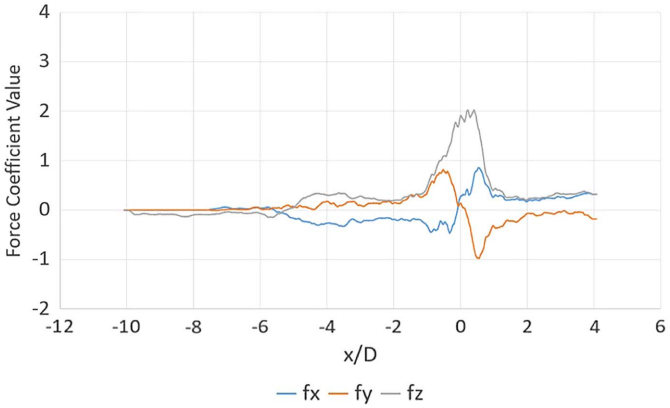

Fig. 11. Time-averaged force coefficients on the small-scaled model of the gable-roofed building versus distance from the center of the vortex to the center of the gable-roofed building model normalized by the core diameter (D).

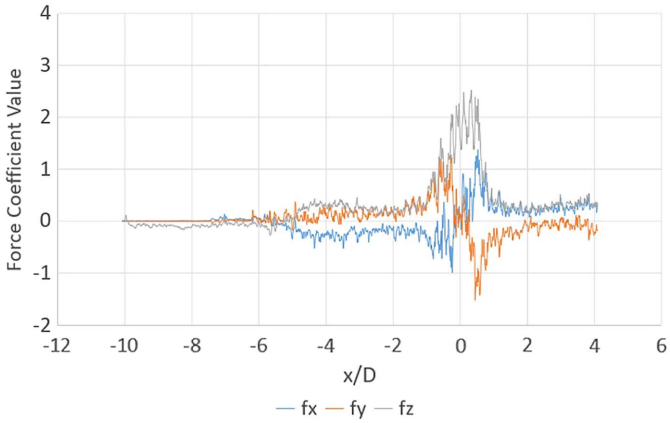

Fig. 12. Force coefficients on the small-scaled model of the gable-roofed building versus distance from the center of the vortex to the center of the gable-roofed building model, x normalized by the core diameter (D). The entire data set is shown. All values are instantaneous.

0.5 s forward. As expected, the averaging process results in a loss of the peak positive and negative values.

To compare the force coefficients from this numerical simulation with the published results [Case 1 in Haan et al. (2010)], the entire data set of Fig. 9 is presented, as shown in Fig. 12. Comparing Fig. 12 to the published experimental results in Haan et al. (2010), the trend of the variation of force coefficients is nearly identical. However, there are some slight differences in peak value that can be seen. The peak instantaneous values are slightly different in the CFD simulation, peak f_z is 0.5 lower, peak f_x is 0.2 higher, and peak f_y is 0.2 higher, which corresponds to 17%, 17%, and 15% difference in f_z, f_x, and f_y, respectively, between the ISU physical simulation and the CFD simulation of the Missouri S&T facility. This serves to validate the CFD simulation results and justifies further exploration of the simulation results.

Revealing Bluff-Body Aerodynamics on Low-Rise Buildings under Tornado-Like Vortices

To understand how the presence of a low-rise building alters the flow pattern and the velocity field near the ground and near the building, and to determine the pressure distribution on the building surface when the tornado vortex passes by the building model, three representative instances are studied and the related results are presented in the following sections. For each instance, tangential velocity, resultant velocity, flow pattern around the building model in terms of streamlines, and pressure coefficients on the surface of the building model and pressure coefficients around the building in the wind field are investigated. As the ground plane boundary conditions remained the same as the tornado translated, the core radius remained around 0.27 m with some slight variation. Comparing this dynamic behavior of the core radius to time-averaged, the time-averaged core radius would be relatively stable. As such, core radius comparison was not deeply investigated.

Velocity Field, Flow Pattern and Pressure Distribution on Structural Surface when the Building is Subjected to the Maximum Force in the Z-Direction

When the center of the vortex has passed the building model's center, but the building model is still inside of the core radius, as shown in Fig. 13, the building is subjected to the maximum force

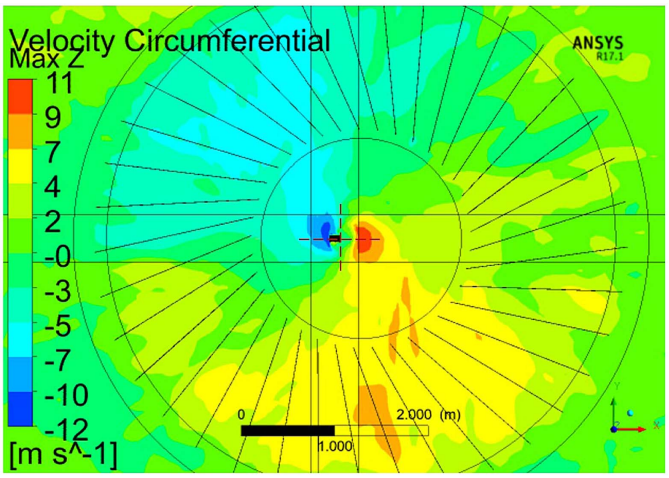

Fig. 13. Relative location between the center of the tornado vortex and the center of the building model when the building is subjected to the maximum force in the z-direction. The dashed cross indicates the center of the vortex.

in the *z*-direction (axes specified in Fig. 1). Fig. 14 presents streamlines, resultant velocity, and pressure around the building on the horizontal plane at the elevation of 0.038 m, just below the eave height (0.041 m). From the streamlines around the building, as shown in Fig. 14(a), the wind impacts the building model Wall AB perpendicularly, making it like a windward wall. However, the wind velocity varies along the width of the windward wall, which is different from straight-line wind (Tominaga et al. 2015; Gierson et al. 2017; Duthinh et al. 2018). Once the air flow reaches the windward wall, it mainly passes the building along one side (Wall AD), which again is different from straight-line wind. Due to the presence of the building model, the streamlines converge and thus the velocity increases based on the mass continuity theorem, evidenced by higher velocity region to the left of the building in Fig. 14(b). Consequently, the increase in velocity results in a decrease in pressure based on Bernoulli's theorem, leading to negative pressure on Wall AD. In addition, when the air flow passes the sharp corner (Corner A), boundary layer separation occurs, generating vortex shedding and accordingly increasing the negative pressure at Corner A locally, which explains the higher value of negative pressure at Corner A locally, as shown in Fig. 14(c). On Wall AD, close to Corner D, due to the convergence of tornadic wind flow, air flow attacks this part of the wall, plus the flow reattachment of flow separation at Corner A, leading this part of Wall AD to also behave like a windward wall. When the air flow passes Corner D, streamlines converge, and thus velocity increases based on mass continuity theorem, which is evidenced by the darker region around Corner D in Fig. 14(b). Due to the wind angle of attack on this part of Wall AD, flow separation does not occur at Corner D and thus the no local higher negative pressure area is spotted at Corner D. It is noted that Bernoulli's theorem may not be rigorously applicable in a rotation flow, it is consistent with the obtained results. Further theoretical research may be needed to develop a rigorous theorem to explain bluff-body aerodynamic in rotating wind flow. The negative pressure on Walls BC and CD is caused by the atmospheric pressure drop in the vortex core region. From Fig. 14(c), the pressure on Walls AD and BC is not symmetric. Although the pressure on both walls is negative, the magnitude of the pressure on Wall BC is much higher than that on Wall AD, leading the total force in the x-direction (axes specified in Fig. 1) to point to the right, toward the center of the vortex.

Fig. 15 presents streamlines, resultant velocity, and pressure around the building on a horizontal plane at an elevation of 0.0575 m (i.e., mean roof height). By comparing Figs. 14(a) and 15(a), the tornadic flow varies along the height, the core becomes bigger at the elevation of 0.0575 m than that at the elevation of 0.038 m. The velocities at the mean roof height on the far roof are nearly zero, as shown in Fig. 15(b), which is due to the low velocity at the core region. In Fig. 15(b), higher velocity regions (velocity acceleration) on the two sides of Point E can be explained due to the streamline convergence when the air flow passes over the roof and the left wall (Side EH), based on the mass continuity theorem. In Fig. 15(c), the negative pressure around the building is due to the significant atmospheric pressure drop.

From Fig. 16, all pressure on the building surface is negative, even on the windward wall (Wall AB). This is because the building model is inside the vortex core and significant atmospheric pressure drop dominates the pressure environment around the building. However, on the windward wall, the negative pressure is reduced due to the perpendicular attacking of the air flow. On Wall BC (side wall), the pressure distribution is uniform, while the pressure distribution on Wall AD is not uniform due to the flow separation at Corner A, flow reattachment, and direct flow attacking. This results in the asymmetrical pressure on the two side walls, leading to a

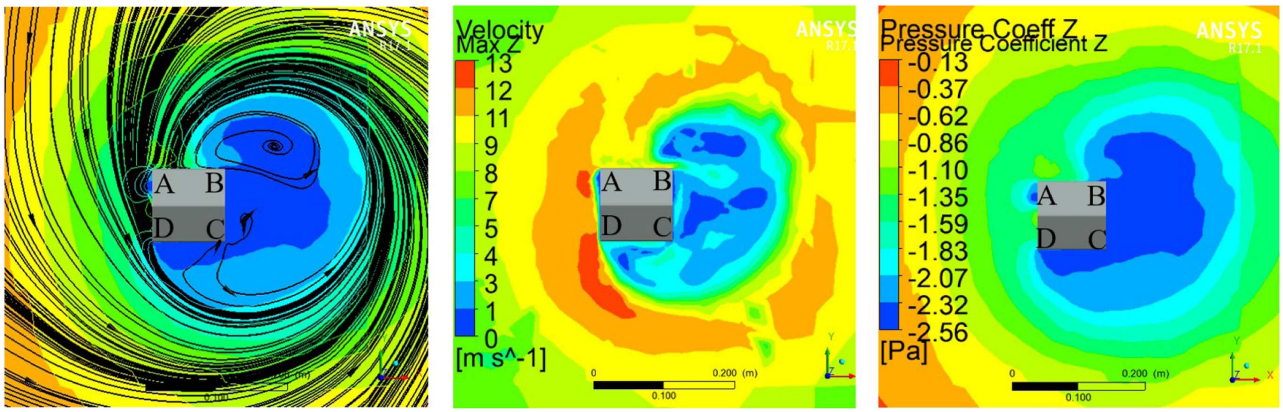

(a) (b) (c)

Fig. 14. Streamlines, velocity field, and pressure field on the horizontal plane at the elevation of 0.038 m, just below eave height, when the building is subjected to the maximum force in the z-direction: (a) streamlines around the building model with contours of pressure coefficient [from (c)]; (b) resultant velocity field around the building model; and (c) pressure contours around the building model.

J. Struct. Eng., 2022, 148(3): 04021294

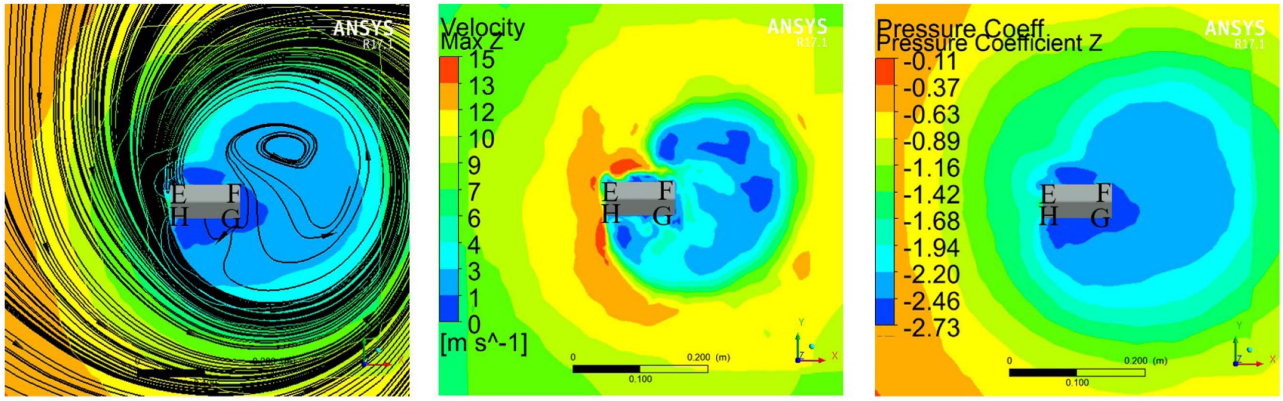

Fig. 15. Streamlines, velocity field, and pressure field on the horizontal plane at the elevation of 0.0575 m, mean roof height, when the building is subjected to the maximum force in the z-direction: (a) streamlines around the building model with contours of pressure coefficient [from (c)]; (b) resultant velocity field around the building model; and (c) pressure contours around the building model.

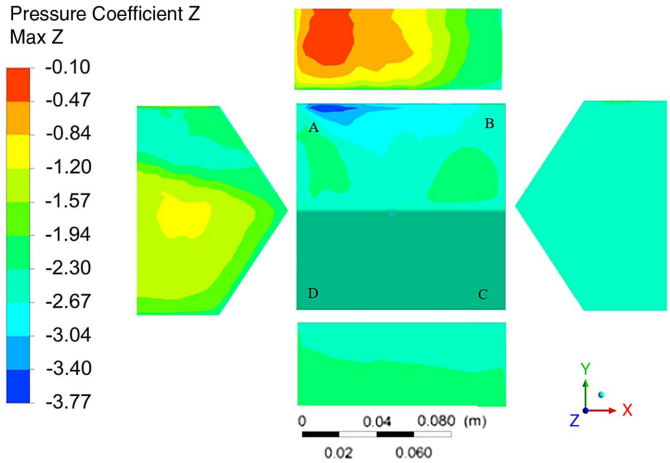

Fig. 16. Pressure distribution on the surface of the building model when the building is subjected to the maximum force in the z-direction.

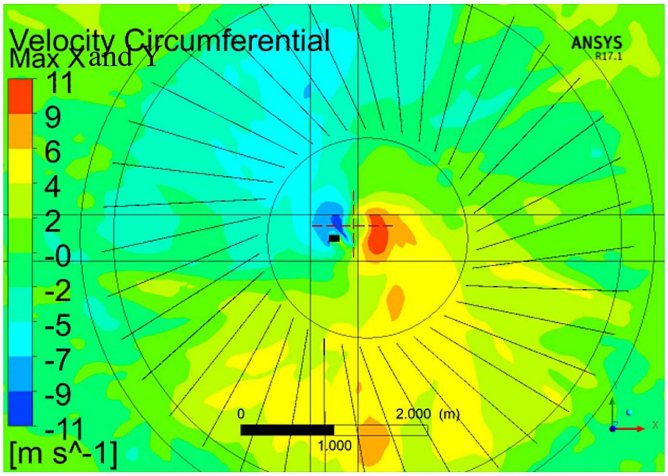

Fig. 17. Relative location between the center of the tornado vortex and the center of the building model when the building is subjected to the maximum force in the x- and y-directions (when the vortex center has passed the building model). The dashed cross indicates the center of the vortex.

significant total force in the x-direction (axes specified in Fig. 1) pointing to the tornado center. In fact, under tornadic winds, although the total force in the x-direction varies with location/time, it always points to the tornado center, indicating that the tornado tries to suck the building model to its center. On the contrary, under straight-line winds, the pressure on the two side walls is almost the same, leading the total force in the across-wind direction to be so small as to be negligible. On the windward roof (close Corner A), the negative pressure is increased due to the flow separation at the sharpened corners. The peak negative pressure occurs on the windward roof, with a coefficient of −3.77. The majority of the roof, Wall CD, and Wall BC have pressure coefficients ranging from −1.94 to −3.04.

Velocity Field, Flow Pattern and Pressure Distribution on Structural Surface when the Building is Subjected to the Peak Forces in the X- and Y-Directions

At the location of the maximum force in the x-and y-directions, after the center of the vortex has passed the building

When the center of the vortex has passed the building model's center, and the building model is at the core radius, as shown in Fig. 17, the building is subjected to the maximum force in the x- and y-directions (axes specified in Fig. 1). Fig. 18 presents streamlines, resultant velocity, and pressure around the building on the horizontal plane at the elevation of 0.038 m, just below eave height (0.041 m). The angle of wind attack on the building model is about 45°. This angle facilitates the flow in passing Wall AB and Wall AD, without flow separation. After Corners B and D, the streamlines converge due to the blockage of the building, and accordingly, the velocity around the building increases based on the mass continuity theorem, as indicated by the higher velocity locations, as shown in Fig. 18(b). Based on Bernoulli's theorem, whereby increases in velocity result in decreases in pressure, the increase in velocity around Corners B and D of the building results in a decrease in pressure, that is, the relative pressure at around Corners B and D is negative, indicated in Fig. 18(c). In addition, after the air passes Corners B and D, velocity becomes zero indicating that boundary layer separation occurred at Corners B and D, which are sharp. Near Corner C, the maximum negative pressure

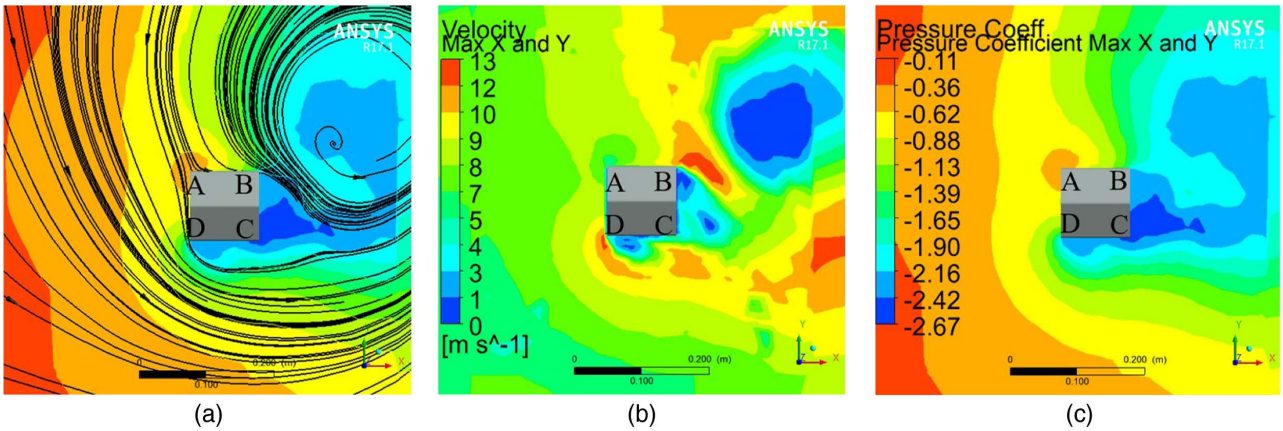

Fig. 18. Streamlines, velocity field, and pressure field on the horizontal plane at the elevation of 0.038 m, just below eave height, when the building is subjected to the maximum force in the x- and y-directions (when the vortex center has passed the building model): (a) streamlines around the building model with contours of pressure coefficient [from (c)]; (b) resultant velocity field around the building model; and (c) pressure contours around the building model.

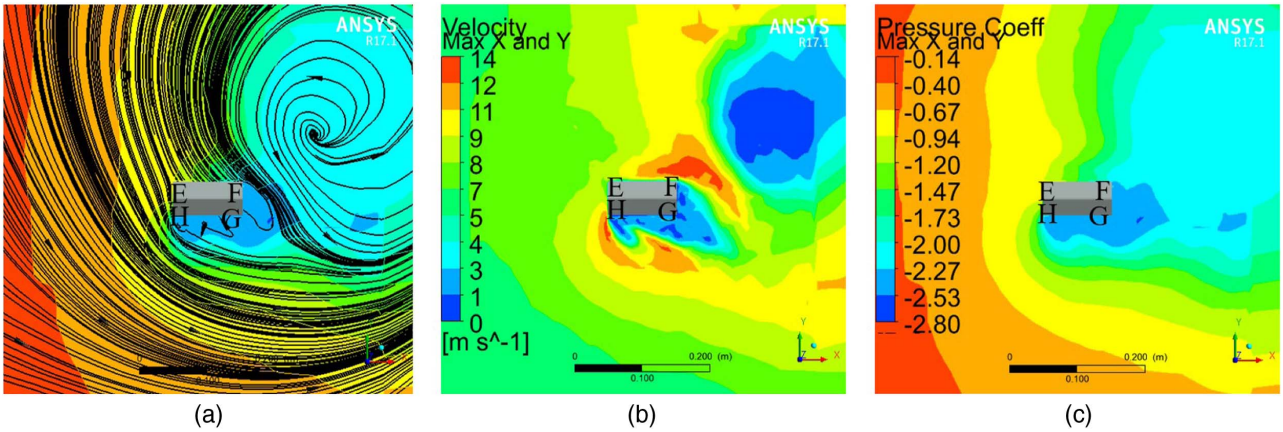

Fig. 19. Streamlines, velocity field, and pressure field on the horizontal plane at the elevation of 0.0575 m, mean roof height, when the building is subjected to the maximum force in the x- and y-directions (when the vortex center has passed the building model): (a) streamlines around the building model with contours of pressure coefficient [from (c)]; (b) resultant velocity field around the building model; and (c) pressure contours around the building model.

coefficient is found in the vicinity of the building model, −2.67, shown in Fig. 18(c). This is due to the significant atmospheric pressure drop inside the tornado core.

Fig. 19 presents streamlines, resultant velocity, and pressure around the building on a horizontal plane at an elevation of 0.0575 m, the mean roof height. Comparing Figs. 19(a) and 18(a), the density of streamlines is different, indicating the variation of wind flow along the height. From Fig. 19(a), at a higher elevation, the streamlines are denser, suggesting that the velocity magnitude changes more frequently. Again, the velocity acceleration around Corners F and H can be explained by streamline convergence (mass continuity theorem). Accordingly, in Fig. 19(c), negative pressure around Side FG and Side GH can be explained by Bernoulli's theorem and boundary layer separation.

Fig. 20 shows the pressure on the surface of the building model. Since the majority of the building is still inside the tornado core, negative pressure dominates due to the significant pressure drop. On top of this effect, based on the mass continuity theorem and Bernoulli's theorem as well as boundary layer separation (vortex shedding), on the windward wall, Wall AB and AD, the negative pressure is reduced; on the leeward walls, the negative pressure is

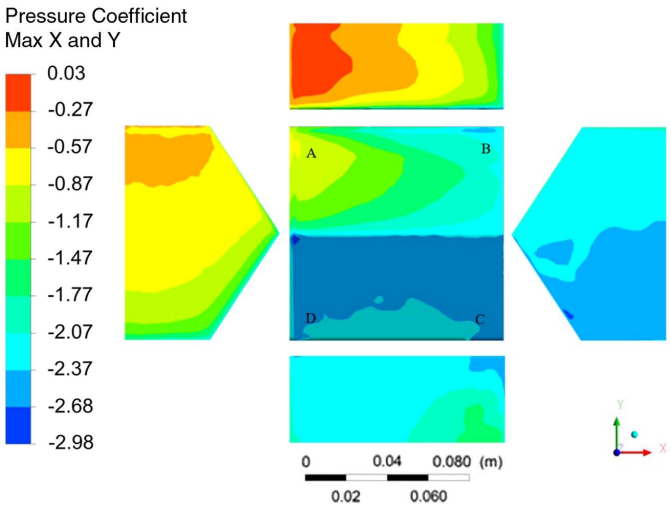

Fig. 20. Pressure distribution on the surface of the building model when the building is subjected to the maximum force in the x- and y-directions (when the vortex center has passed the building model).

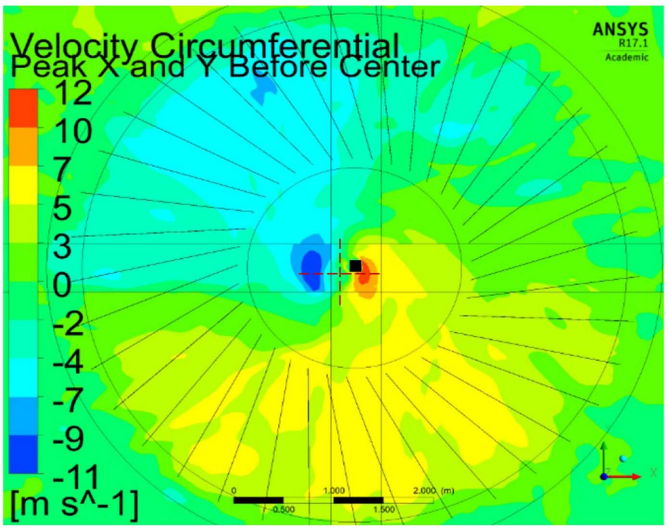

Fig. 21. Relative location between the center of the tornado vortex and the center of the building model when the building is subjected to the peak force in the x- and y-directions before the center of the vortex passes the building model. The dashed cross indicates the center of the vortex.

increased. In terms of this, the tornadic wind field has some similarities to a straight-line wind field. The pressure coefficients on Walls BC and CD are lower than the rest of the building due to vortex shedding. Along the wind blowing direction to the building, the wind pressure direction is not symmetrical along this direction, which is different from the effect of straight-line wind. Again, in the *x*-direction, the total force points to the right, indicating that the tornado sucks the building toward the vortex center. The highest pressure coefficient is −2.98, which occurs at the roof corner and wall corner due to boundary layer separation and vortex shedding. The majority of the roof has pressure coefficient values that range from −1.17 to −2.68.

At the location of the other peak in the x- and y-directions, before the center of the vortex has passed the building

When the center of the vortex has not yet passed the building model's center, and the building model is at the core radius (the vortex core radius passes the building model the first time), as shown in Fig. 21, the building is subjected to the first peak in force in the *x*- and *y*-directions (axes specified in Fig. 1). Fig. 22 presents streamlines, resultant velocity, and pressure around the building on a horizontal plane at an elevation of 0.038 m, just below eave height (0.041 m). In this instance, Wall DC can be considered as the windward wall. Wind velocity varies along the length on the windward wall and the wind's angle of attack is about 15 degrees. The velocity acceleration around Corners B, D, and C in Fig. 22(b) can be explained by streamline convergence, as shown in Fig. 22(a). Boundary layer separation and vortex shedding are observed at Corners D and B. The negative pressure around Walls AB and AD is mainly caused by the atmospheric pressure drop at the tornado core.

Fig. 23 presents streamlines, resultant velocity, and pressure around the building on a horizontal plane at an elevation of 0.0575 m, mean roof height. From Fig. 23(a), wind first impacts Corner G at this elevation, indicating that wind blowing direction changes along elevation. Then, the wind mainly passes along Side GH, causing the streamlines to converge and thus causing the pressure to reduce [negative pressure in Fig. 23(c) below Side GH is associated with the high velocity contour in Fig. 23(b)]. In Fig. 23(c), the negative pressure around Sides EF and EH is mainly caused by the significant atmospheric pressure drop.

Fig. 24 shows the pressure on the surface of the building model. At this location, the pressures on the building are all negative due to the proximity to the center of the vortex. Again, on the windward wall, the negative pressure magnitude is reduced. The highest negative pressure, −3.49, is observed at the corner of the roof, where the boundary layer separation and vortex shedding occur. Again, the pressures on the left and right walls are not symmetrical. This leads to a total force pointing to the left, toward the tornado-like vortex center. The force in the *x*-direction (axes specified in Fig. 1) always points toward the vortex center.

The primary difference between the results for the two instances where the peaks in the *x* and *y* forces are found include higher velocities occurring on opposite corners of the building at the peak location after the vortex center passes, Fig. 18(b), lower pressure coefficient values occurring behind the building (relative to the direction of the streamlines), Fig. 18(c), and streamlines impacting the building at a roughly 45-degree angle of attack, Fig. 18(a). Before the vortex center passes, Figs. 22(a–c), the velocity on opposing

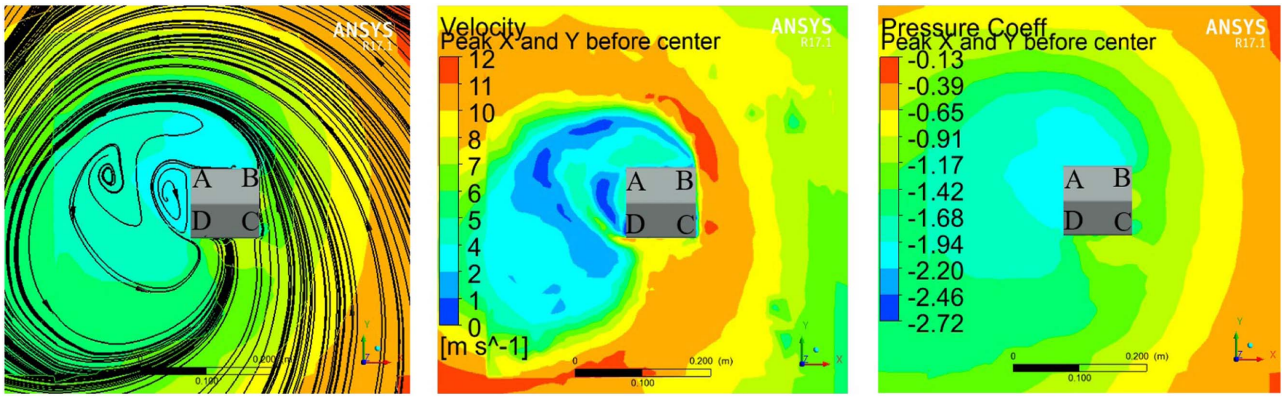

(a) (b) (c)

Fig. 22. Streamlines, velocity field, and pressure field on the horizontal plane at the elevation of 0.038 m, just below eave height, when the building is subjected to the peak force in the x- and y-directions before the center of the vortex passes the building model: (a) streamlines around the building model with contours of pressure coefficient [from (c)]; (b) resultant velocity field around the building model; and (c) pressure contours around the building model.

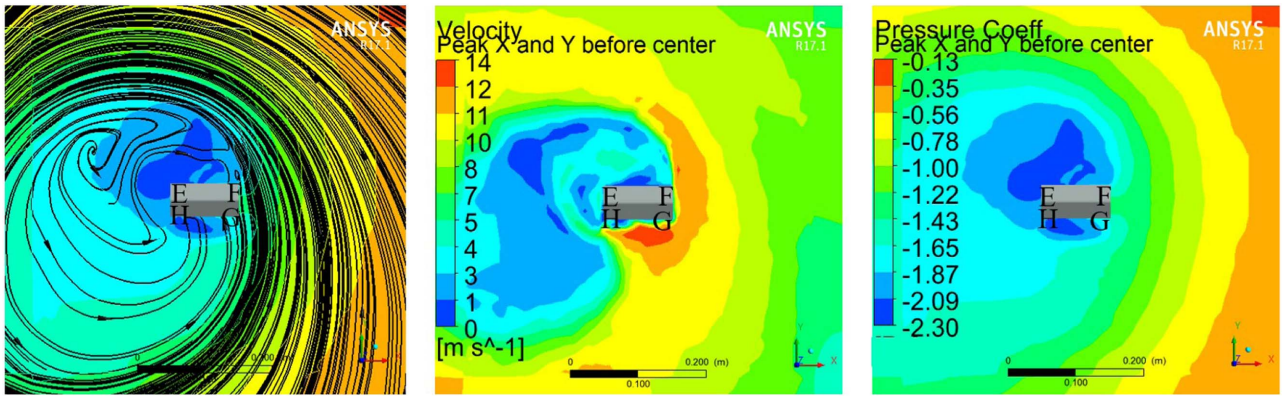

Fig. 23. Streamlines, velocity field, and pressure field on the horizontal plane at the elevation of 0.0575 m, mean roof height, when the building is subjected to the peak force in the x- and y-directions before the center of the vortex passes the building model: (a) streamlines around the building model with contours of pressure coefficient [from (c)]; (b) resultant velocity field around the building model; and (c) pressure contours around the building model.

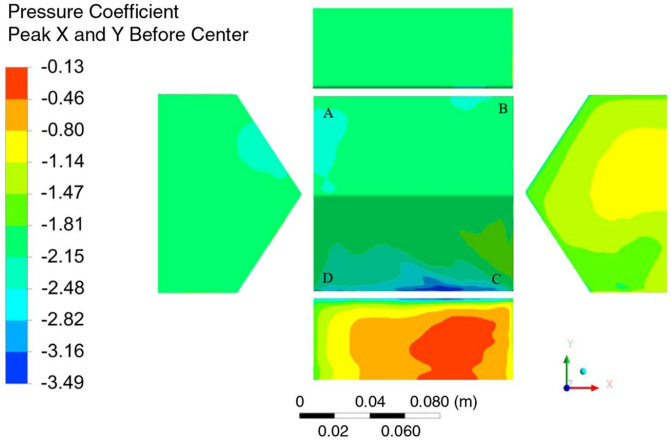

Fig. 24. Pressure distribution on the surface of the building model when the building is subjected to the peak force in the x- and y-directions before the center of the vortex passes the building model.

corners is lower, the pressure behind the building is not as negative, and the streamlines appear to impact the building at a perpendicular angle. Comparing Figs. 19 and 20 to Figs. 23 and 24, the previous findings are reinforced at higher elevations around the building and on the building surface. Table 2 summarizes some of these comparisons. However, in both situations, the mass continuity theorem and Bernoulli's theorem are still applicable. In addition to this, after the vortex center passes the building model, the flow around the building appears to be more symmetrical, having vortex shedding at opposite corners of the structure, whereas at the location before the vortex center passes the building model, the vortex shedding is asymmetrical due to the fact that the building model is located between core radius and vortex center, where the flow is more turbulent.

Conclusions

In this study, CFD simulation is applied to model the entire process of experimental testing of a low-rise building model in the large-scale physical tornado simulator, where the swirling wind flow produced in the tornado simulator translates over the building model. The developed CFD model is validated using the published testing results from (Haan et al. 2010). Through CFD simulation, the behavior of the wind field around the building model can be easily obtained in higher resolution than physical testing. To explore the bluff-body aerodynamic of low-rise buildings under tornadic winds, the streamlines, velocity field, and pressure field as well as the surface pressure on the building model are extracted when the swirling wind flows moves to some representative locations, i.e., locations at which the maximum forces in the *x*-, *y*-, and *z*-direction (axes specified in Fig. 1) are observed. The following conclusions are drawn:

- Flow velocity, and thereby pressure, varies along the wall width (along the radial distance in this study), which is different from straight-line winds (Tominaga et al. 2015; Gierson et al. 2017; Duthinh et al. 2018). Under straight-line winds, velocities along the wall width are uniform at the same elevation.
- Tornadic wind flow is indeed 3D flow, which is evidenced by the variation in the behavior and density of streamlines along the

Table 2. Summary comparison of results from locations of peak forces in the *x*- and *y*-directions

Expression	Before vortex center passes	After vortex center passes
Maximum pressure Coefficient around building	−0.65	−0.36
Minimum pressure Coefficient around building	−1.94	−2.67
Peak velocity at Corner "A"	2 m/s (4.47 mph)	8 m/s (17.9 mph)
Peak velocity at Corner "B"	12 m/s (26.8 mph)	13 m/s (29.1 mph)
Peak velocity at Corner "C"	10 m/s (22.4 mph)	7 m/s (15.7 mph)
Peak velocity at Corner "D"	11 m/s (24.6 mph)	13 m/s (29.1 mph)
Wind angle of attack	~0°	~45°
Maximum pressure coefficient on building surface	−0.13	−0.03
Minimum pressure coefficient on building surface	−3.49	−2.98

height of the building and at different locations on the same horizontal plane.

- The mass continuity theorem and Bernoulli's theorem can be applied to explain the data by relating streamline convergence, to increase in velocity, and further to decrease in pressure, at least qualitatively. Since Bernoulli's theorem theoretically does not apply to rotational flow, future work is suggested on the theoretical derivation and/or numerical quantification of the relationship among streamline pattern change, velocity change, and pressure change.
- Boundary layer separation and vortex shedding occur on and near the building under tornadic winds, which is similar to the situation under straight-line winds.
- Forces on the two side walls of the building are not symmetric under tornadic winds, which causes F_x to always point toward the center of the vortex.

Validated numerical simulation of the entire process of physical testing in tornadoes simulators will alleviate the demands associated with high volume physical lab testing. To determine design tornadic wind loading, future systematic numerical simulations of physical testing can be conducted on a variety of scenarios. This will allow for modification of the coefficients of Kz, Kzt, Kd, Ke, G, and Cp in the pressure equation specified in ASCE 7-16, with CFD simulation of the actions of the equivalent straight-line winds for comparison. For example, if structures with different archetypes are "tested" numerically using the developed CFD models, guidance on the modification of C_p can be obtained. As design against low-intensity tornadoes has been justified (Kuligowski et al. 2014) in order to reduce the damage and economic loss to the entire community as a whole for a certain period, the developed "numerical" tornado simulator will be promising to generate sufficient data to help ASCE7 determine design tornadic wind loading at a low cost.

Data Availability Statement

All data, models, and code generated or used during the study appear in the published article.

Acknowledgments

The authors greatly appreciate the financial support from the VORTEX-SE Program within the NOAA/OAR Office of Weather and Air Quality under Grant No. NA20OAR4590452 and the financial support from National Science Foundation, through the project, "Damage and Instability Detection of Civil Large-scale Space Structures under Operational and Multi-hazard Environments" (Award No. 1455709), and two other projects (Nos. 1940192 and 2044013).

References

Changnon, S. A. 2009. "Tornado losses in the United States." *Nat. Hazard. Rev.* 10 (4): 145–150. https://doi.org/10.1061/(ASCE)1527-6988(2009)10:4(145).

Duthinh, D., J. A. Main, M. L. Gierson, and B. M. Phillips. 2018. "Analysis of wind pressure data on components and cladding of low-rise buildings." *J. Risk Uncertainty Eng. Syst. Part A: Civ. Eng.* 4 (1): 04017032. https://doi.org/10.1061/AJRUA6.0000936.

Fluent Manual. 2017a. *Large eddy simulation*. Canonsburg, PA: ANSYS.

Fluent Manual. 2017b. *Sliding mesh technique*. Canonsburg, PA: ANSYS.

Gierson, M. L., B. M. Phillips, D. Duthinh, and B. M. Ayyub. 2017. "Wind-pressure coefficients on low-rise building enclosures using modern wind-tunnel data and Voronoi diagrams." *J. Risk Uncertainty Eng. Syst. Part A: Civ. Eng.* 3 (4): 04017010. https://doi.org/10.1061/AJRUA6.0000915.

Haan, F. L., V. K. Balaramudu, and P. P. Sarkar. 2010. "Tornado-induced wind loads on a low-rise building." *J. Struct. Eng.* 136 (1): 106–116. https://doi.org/10.1061/(ASCE)ST.1943-541X.0000093.

Haan, F. L., P. P. Sarkar, and W. A. Gallus. 2008. "Design, construction and performance of a large tornado simulator for wind engineering applications." *Eng. Struct.* 30 (4): 1146–1159. https://doi.org/10.1016/j.engstruct.2007.07.010.

Kuai, L., F. L. Haan, W. A. Gallus, and P. P. Sarkar. 2008. "CFD simulations of the flow field of a laboratory-simulated tornado for parameter sensitivity studies and comparison with field measurements." *Wind Struct.* 11 (2): 75–96. https://doi.org/10.12989/was.2008.11.2.075.

Kuligowski, E. D., F. T. Lombardo, L. T. Phan, M. L. Levitan, and D. P. Jorgensen. 2014. "Final report, national institute of standards and technology technical investigation of the May 22, 2011, Tornado in Joplin, Missouri." *Nat. Inst. Stand. Technol.* 22 (May): 1–494. https://doi.org/10.6028/NIST.NCSTAR.3.

Liu, Z., and T. Ishihara. 2015. "A study of tornado induced mean aerodynamic forces on a gable-roofed building by the large eddy simulations." *J. Wind Eng. Ind. Aerodyn.* 146 (Nov): 39–50. https://doi.org/10.1016/j.jweia.2015.08.002.

Mishra, A. R., D. L. James, and C. W. Letchford. 2008. "Physical simulation of a single-celled tornado-like vortex, part B: Wind loading on a cubical model." *J. Wind Eng. Ind. Aerodyn.* 96 (8): 1258–1273. https://doi.org/10.1016/j.jweia.2008.02.027.

NOAA (National Oceanic and Atmospheric Administration). 2019. "The national severe storms laboratory of national oceanic and atmospheric." Accessed November 21, 2019. http://www.nssl.noaa.gov/education/svrwx101/tornadoes/.

Rajasekharan, S. G., M. Matsui, and Y. Tamura. 2013. "Characteristics of internal pressures and net local roof wind forces on a building exposed to a tornado-like vortex." *J. Wind Eng. Ind. Aerodyn.* 112 (Jan): 52–57. https://doi.org/10.1016/j.jweia.2012.11.005.

Refan, M., and H. Hangan. 2016. "Characterization of tornado-like flow fields in a new model scale wind testing chamber." *J. Wind Eng. Ind. Aerodyn.* 151 (Apr): 107–121. https://doi.org/10.1016/j.jweia.2016.02.002.

Simmons, K. M., D. Sutter, and R. Pielke. 2013. "Normalized tornado damage in the United States: 1950–2011." *Environ. Hazards* 12 (2): 132–147. https://doi.org/10.1080/17477891.2012.738642.

Snyder, J. C., and H. B. Bluestein. 2014. "Some considerations for the use of high-resolution mobile radar data in tornado intensity determination." *Weather Forecasting* 29 (4): 799–827. https://doi.org/10.1175/WAF-D-14-00026.1.

Tominaga, Y., S. Akabayashi, T. Kitahara, and Y. Arinami. 2015. "Air flow around isolated gable-roof buildings with different roof pitches: Wind tunnel experiments and CFD simulations." *Build. Environ.* 84 (Jan): 204–213. https://doi.org/10.1016/j.buildenv.2014.11.012.

Yuan, F., G. Yan, R. Honerkamp, K. M. Isaac, M. Zhao, and X. Mao. 2019. "Numerical simulation of laboratory tornado simulator that can produce translating tornado-like wind flow." *J. Wind Eng. Ind. Aerodyn.* 190 (Jul): 200–217. https://doi.org/10.1016/j.jweia.2019.05.001.